ASEAN Engineering Journal

Full Paper

CIRCULAR TUNNEL STRUCTURAL ANALYSIS IN SOFT GROUND

Poi Ngian Shek[a]*, Ze Yang Lee[b]

[a]Construction Research Centre (CRC-UTM), Universiti Teknologi Malaysia, 81310 UTM Johor Bahru, Johor, Malaysia
[b]Faculty of Civil Engineering, Universiti Teknologi Malaysia, 81310 UTM Johor Bahru, Johor,Malaysia

Article history
Received
02 March 2022
Received in revised form
30 May 2022
Accepted
29 June 2022
Published online
28 February 2023

*Corresponding author
shekpoingian@utm.my
r

Graphical abstract

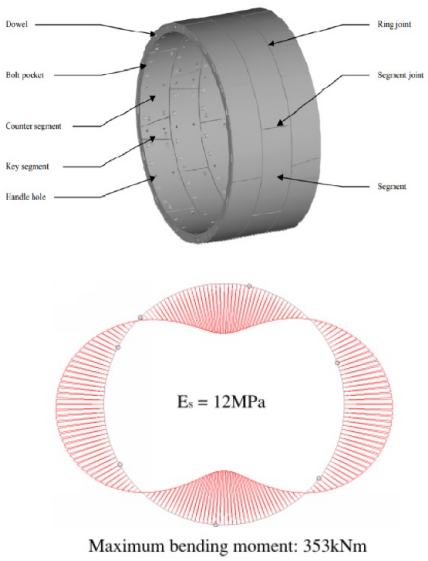

Abstract

Analytical bedded-beam spring model is most commonly adopted in the tunnel engineering practice due to its simplicity and promising outputs. Despite many well documented literatures exist concerning about the theories and fundamentals of various methods, there is a dearth of information on the modelling framework of a bedded-beam spring and many details are often overlooked in the modelling process. The main aim of this paper is to produce the modelling framework of the bedded-beam spring model in soft ground, for both direct and indirect approaches in considering the effects of segmental joints. Particular emphasis is devoted to the modelling techniques of each components of the structural model which in turn, is able to facilitate the modelling quality and process for the practicing engineers. Reviews on the technical papers of tunneling variables as well as parameters identification for the structural analysis have been first performed followed by the comparison of the consideration adopted in the modelling techniques. Analyses have been carried out to evaluate the structural forces on the tunnel lining and the obtained results are discussed in a comparison with the field measurements and design values of the actual tunneling projects. The results suggested that the direct approach always yields greater bending moments up to i) 26% for 6+1 ring configuration and ii) 21% for 5+1 ring configuration compared to that of the indirect approach. With the presence of more number of radial joints, the differences between the approaches have the tendency to be greater. With the validated models, parametric studies including tunnel lining flexibility ratio, compressibility ratio and the soil lateral earth pressure coefficient have been performed to provide better insight on the relative importance of each of the parameters. The results of the studies suggested that with the increase in flexibility ratio, the difference between the direct and indirect approach has shown to increase from 10% to 28%. However, insignificant influence has been observed on the axial forces regardless of the joint consideration approach a well as the compressibility ratio.

Keywords: Bedded-beam spring model, radial joints, modeling framework

1.0 INTRODUCTION

Modern urban development around the world has made shield tunneling technology to be developed extensively. Tunneling shield acts as the temporary supporting structure during the excavation of soil carried out by tunnel boring machine (TBM) before the permanent support structure, the tunnel segmental lining is installed. A circular shield driven tunnel is generally made up of a certain number of precast segmental concrete segments that will be assembled at the radial joints to form a ring called segmental lining [1]. The calculation models of tunnel design have been developed since 1926. In the tunneling industry, significant amount of computational time and resources can be taken to perform the three-dimensional (3D) finite element analysis. Hence, the segmental linings are usually evaluated in simplified two-dimensional (2D) schemes by 2 approaches, either continuum based or beam-based approach, within which the methods proposed by Duddeck and Erdmann [2] have been

widely used. A summary of the structural models proposed by the authors are tabulated in Table 1.

Table 1 Glossary and evolution of structural design models for tunnel

Authors	Description or other comments
Schmid [3]	Theory of elastic continuum model considering soil-lining interaction for thick lining
Voellmy [4]	Elastic continuum model (omits tangential shear stress transmission)
Morgan [5]	Analytical solution of continuum models considering elliptical deformation of tunnel lining (omits tangential shear stress transmission)
Schulze and Duddeck [6]	Bedded-beam spring model for shallow tunnels (omits bedding at tunnel crown)
Windels [7]	Extension of Schulze and Duddeck (considers geometrical non-linearity)
Windels [8]	Analytical solutions of full slip and full bond elastic continuum model (considers geometrical non-linearity and pre-deformation)
Muir Wood [9]	Correction on elliptical deformation mode of Morgan (1961) by considering the tangential components (omits radial deformation due to tangential stress)
Muir Wood [10]	Inclusion of radial deformation due to tangential stress
Duddeck and Erdmann [11]	Continuum model for deep tunnel (cover-to-diameter ratio, C/D $\geq$ 2) and bedded-beam spring model for shallow tunnels without ground pressure reduction at crown (cover-to-diameter ratio, C/D $\leq$ 3)
Blom [12]	Inclusion radial joints and soil reactions on tunnel deformation mode
Oreste [13]	Estimation of tunnel segmental lining internal forces in rock using finite element method (FEM)
Ngan Vu, et al. [14]	Bedded-beam spring model for shallow tunnels with ground pressure reduction at tunnel crown

1.1 Two Dimensional (2D) Analytical Methods For Segmental Lining Design

The continuum-based approach, derived from the theory of elasticity, regards the tunnel to be bedded in an infinite elastic medium and the ring forces could be determined by closed form solutions. The continuum approach assumes tunnel as a thin ring bedded in infinite elastic space which is suitable for the evaluation of structural forces of deep tunnels (overburden is greater than two time its diameter). Within the solution, two possible extreme cases are considered: (i) Full-slip; (ii) no-slip (full bond). Full-slip condition neglects the tangential component: frictional bond between the soil and the ring. This condition is commonly adopted to evaluate the maximum bending moments and shear forces in the ring [11]. Under this condition, shear stress transmission between the soil-structure interface is non-existent, which is only applicable when tunnel is in soft soil medium or surrounded by soft tail grouting. Thus, the continuity of stresses and displacements in the tangential component are not met. In contrast, under full bond condition, the tangential components of soil pressures transferred to the tunnel lining as friction bonds are considered and this considers continuity of stresses as well as displacements at the soil structure interface.

Beam-based approach, also known as action-reaction model (Figure 1) considers the tunnel as a bedded-beam spring model whereby the ground is simulated as individual bedding springs to represent the coupling conditions between tunnel lining and the ground [15]. The supporting effects provided by the surrounding soil are simulated as compression only radial springs. The frictional components between the soil structure interface are represented by tangential springs. With this approach, the influence of segmental radial joints could be considered. In the literature, there are generally two methods in considering the presence of segmental radial joints in the bedded-beam spring model known as indirect-joint and direct-joint models [16]. The indirect method proposed by Muir Wood [9] regards the segmental lining as a monolithic ring with reduced lining rigidity in considering the effect of joints. As for the direct-joint models, the segmental tunnel lining is perceived as a ring with multi-hinge with rotational stiffness. Although these methods are commonly used in practice, there are limited research on the differences and relationships between them due to the extensive amount of design parameters. Generally, beam-based approach proposed by Duddeck and Erdmann [11] without bedding at the tunnel crown is suitable for shallow tunnel with overburden less than three times its diameter.

The specific advantages of the beam-based analytical approach in comparison to continuum-based approach are its versatility in analyzing additional variables such as heterogenous soil condition, non-uniform load application, joints consideration, which are not included in the continuum model [17].

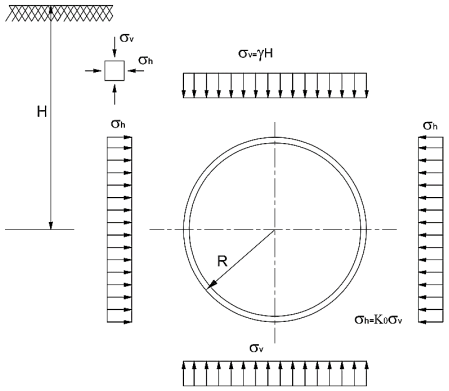

(a)

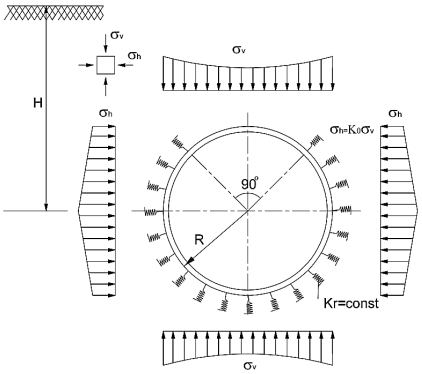

(b)

Figure 1 Representation of tunnel lining analytical model a) continuum model b) bedded-beam spring model [11]

Over the past half century, tremendous efforts have been pertaining to the technical aspects of numerical modelling of the tunnel segmental lining which however, the fact that numerical models and 3D finite element analysis are not always implemented in the projects of the engineering industry. In fact, 2D bedded-beam spring model have been widely used in most of the tunneling projects around the world. The modelling framework of 2D bedded-beam spring structural model development is often generic deliberately due to confidentiality reasons and thus, the framework stressing on the accuracy and rigour of models have not been documented. Despite its simplicity, this gap, or disconnection between the researchers and practicing engineers, in many instances, leads to poor and incorrect modelling practice at various stages of structural model construction. Inappropriate modelling and analysis can yield misleading results which are costly to the project stakeholders.

Recognizing this gap in the literature, this paper presents a comprehensive modelling framework of a bedded-beam spring model, covering both technical aspects and modelling aspects to facilitate the modelling process. The tunnel segmental lining design differs in soft ground and rock on how the tunnel interacts with the ground medium and the way the loads are applied. In rock, the tunnel segmental lining is loaded by the overburden from the loosened rock; in soft ground, arching effect of the ground is unlikely and thus, the soil medium deforms and supported by the tunnel lining. Full overburden, that is the total soil mass is usually applied to the tunnel lining, assuming that the active soil stresses will revert to its primary stress state before tunneling has taken place [18]. This paper focuses mainly on the structural behaviour of the tunnel segmental lining in soft ground condition. Validity of the models (indirect-joint model and direct-joint model) are examined through comparison with available field measurements and designed results of actual tunneling projects, i.e. Second Heinenoord Tunnel in Netherland and Ho Chi Minh Metro Line 1 in Vietnam. The presented models are then used for parametric analyses to study the difference in structural behaviour under different design parameters, i.e. lining flexibility ratio, α lining compressibility ratio, β and lateral earth pressure coefficient, K.

2.0 CASE STUDIES

Verification should be performed for the assessment on whether the deterministic models are providing credible outputs. In this study, bedded beam spring models were set up in accordance to the parameters of the case studies. Both the structural behaviour and analytical solutions of the models were verified against the published field data and design results to constitute a validated modelling framework before the models are used for parametric analyses.

2.1 Case Study of Second Heinenoord Tunnel (Reference Project 1)

The construction of Second Heinenoord Tunnel is the first TBM driven tunnel in Netherland (Bakker et al. 2000). The construction started in year 1995 and the tunnel was officially opened in year 1999. The properties of the tunnel are given in Table 2. Field measurements were taken at the North Bank of the river Oude Maas. The tunnel segmental lining was equipped with 10 strain gauges per segment, with all 7 segments instrumented to monitor the stress distribution of the ring. In addition, 2 pressure cells per segment were instrumented on these segments to complement the strain gauges. The measurement of the bending moments and axial forces of the rings taken from the measuring ring at the North Bank on the 9th day and 330th day, with the results obtained from the back-analysis of analytical model and 2D PLAXIS finite element model proposed by Bakker (2003) are shown in Figure 2.

Table 2 Details of reference project 1

Parameter	Symbol	Value	Unit
Tunnel configuration	-	6+1	-
Tunnel external diameter	D	8.28	m
Lining thickness	t	0.35	m
Overburden	H	12.1	m
Lateral earth pressure coefficient	K	0.5	-

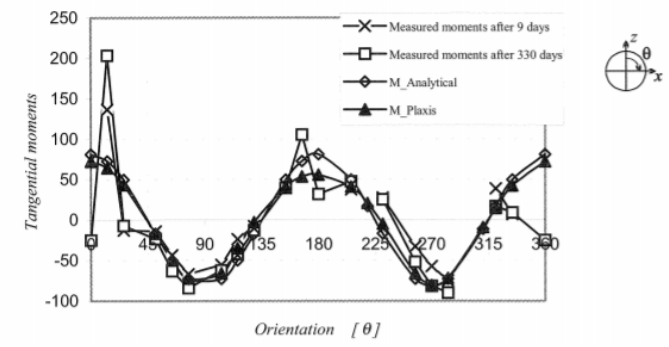

(a)

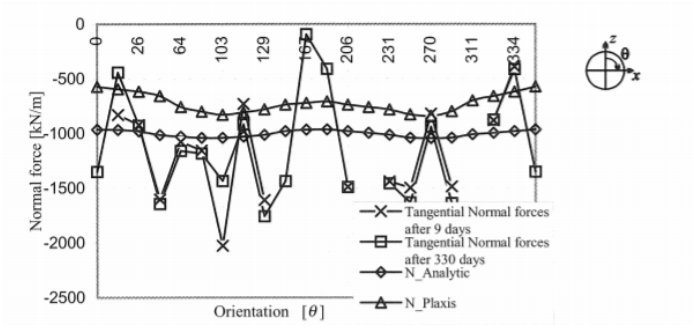

(b)

Figure 2 Comparison of field measured (a) bending moments and (b) normal force with the back-calculation from Bakker [19].

Based on the geological information available, the Second Heinenoord twin bored tunnels at the North Bank of the river Oude Maas were driven through sandy with clay (2), sand with local parts of clay (18) and sand gravel (32) overlain by sand with local parts of clay (3) and mixture of sand and clay (OA/1/OOB) near the ground surface as shown in Figure 3. The ground classification with the corresponding parameters are tabulated in Table 3.

Table 3 Geotechnical parameters of Second Heinenoord Tunnel [20]

Soil identity	Soil type	Bulk density	Effective cohesion	Effective angle of internal friction	Drained modulus
		γ'	C'	ϕ'	E'
		kN/m³	kN/m²	degree	MPa
OA/1/OOB	Mixture of sand and clay	17.2	3	27.0	5.2
3	Sand, local parts of clay	19.5	0	35.0	26.0
2	Sand with clay	19.0	0	33.0	25.0
18	Sand, local parts of clay	20.5	0	36.5	40.0
32	Sand, gravel	20.5	0	36.5	60.0
38A	Clay, local parts of sand	20.0	7	31.0	16.0
38F	Sand	21.0	0	37.5	80.0
38A	Clay, local parts of sand	20.0	7	31.0	16.0

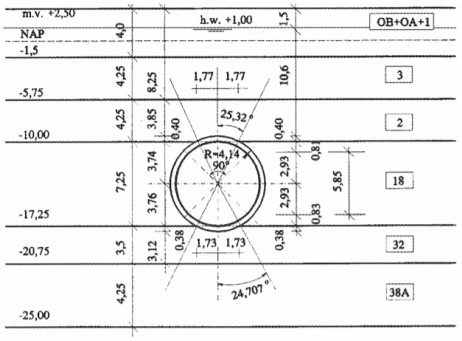

Figure 3 Cross-section of Second Heinenoord Tunnel at the measured location [19, 21]

2.2 Case Study Of Ho Chi Minh Metro Line 1 (Reference Project 2)

The Ho Chi Minh City Metro Line 1 (HCMC MRT Line 1) is the first metro project in HCM city. This MRT line runs from the city centre to Suoi Tien Recreational Park with 2.5 km long being the underground tunneling section and 17.2 km long elevated sections. The properties of the tunnel are given in Table 4. In this project, there was only one measuring location at the east bound tunnel section with the highest building loads located near chainage CH 950. Measuring instruments were installed on the tunnel segments to derive the stress distribution of the tunnel at tunnel crown, axis and invert. Kuriki [22] has included comparison of the design results and obtained field measurements as presented in Figure 4.

Table 4 Details of reference project 2

Parameter	Symbol	Value	Unit
Tunnel configuration	-	5+1	-
Tunnel external diameter	D	6.65	m
Lining thickness	t	0.30	m
Overburden	H	19.8	m
Lateral earth pressure coefficient	K	0.5	-

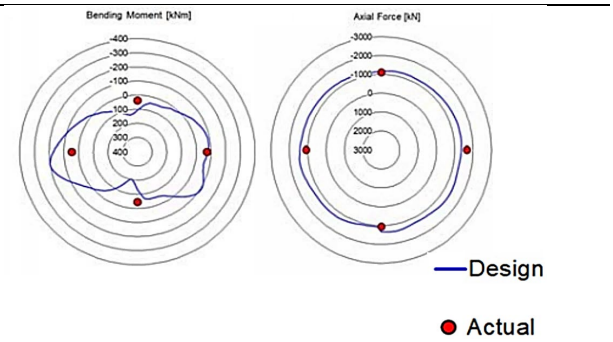

(a) (b)

Figure 4 Comparison of field measured (a) bending moments and (b) normal force with the design values [22]

Based on the geological information available (Figure 5), the HCM twin bored tunnels were excavated through Alluvium Sand

1 (As1) and Alluvium Sand 2 (As2). Table 5 presents the soil layers with the corresponding soil parameters of the project.

Table 5 Geotechnical parameters of Ho Chi Minh Metro Line 1 [22, 23]

Soil identity	Soil type	Bulk density γ' kN/m³	Effective cohesion C' kN/m²	Effective angle of internal friction ϕ' degree	Drained modulus E' MPa
Fill	Fill	19.0	10.0	25.0	10.0
Ac2	Very soft clay	16.5	-	24.0	3.0
As1	Silty fine sand	20.5	0	30.0	12.5
As2	Medium dense to dense sand	20.5	0	33.0	37.5
Dc	Hard to very hard clay	21.0	-	-	85.0
Ds	Dense to very dense sand	20.5	0	35.0	90.0

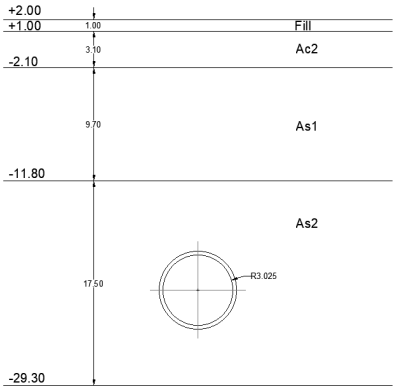

Figure 5 Cross-section of HCM bored tunnel at the measured location [23]

(a)

3.0 ANALYTICAL MODELLING OF BEDDED-BEAM SPRING MODEL

3.1 STAAD. Pro Software

In this study, STAAD Pro has been employed to perform analytical simulations and analysis of the 2D bedded-beam spring model. STAAD Pro is a commercial analysis software that provides flexible user-interface for structural model generation and is widely used in the engineering industry, i.e. design of Randout-West Branch Bypass Tunnel in New York, US. (Brion et al. 2014). The components of the bedded-beam spring model have been created in conjunction with the features in STAAD Pro to implement a modelling framework. The literature review of the modelling techniques using STAAD Pro is given in this section.

3.1.1 Literature review of bedded-beam spring modelling in STAAD Pro

Al-sharafi et al. (2015) presented guidelines of tunnel segmental lining analytical analysis with engineering design process in STAAD Pro. In this study, a bedded-shell spring model was constructed. An overall framework was developed; unfortunately, however, several key elements were not addressed and overlooked that lead to inadequacy of the guidelines. These includes:

1. Huge angle subtended by shell elements
2. Unmeshed shell elements
3. Missing definition of spring stiffnesses and load application methodology
4. Disregard the presence of radial joints
5. Unreasonably high amount of reinforcements designed based on the analysis output

Recently, Adarsh (2018) investigated the structural behaviour of horse-shoe shaped sprayed concrete tunnel in poor rock condition with the bedded-beam spring model. The paper is structured in a way to present a step-by-step modelling guidance of tunnel in STAAD Pro and the commands to generate the model were also included. However, it is worth to note that some elements are not adequately implemented in the model and excluded in the research:

1. Missing application of overburden to the tunnel
2. Utilization of linear analysis (results are the output of the load cases combination which does not reflect the actual behavior of the tunnel under all the load cases in terms of joint displacements, member forces and the soil springs reactions)

In the practicing industry, the engineers rarely opt for 3D shell modelling as significant computation time can be required and likelihood of errors associated with the modelling parameters are higher than the 2D analytical modelling. Important consequences arise from the analysis methods could also lead to erroneous and misleading results. This necessitates the development of a modelling frameworks for the 2D bedded-beam spring model.

3.2 Assumptions Of Bedded-Beam Spring Model In Soft Ground

A bedded-beam spring model takes the reaction resulted from the tunnel lining-ground interaction into account through springs. The commonly applied assumptions for tunnel design in soft ground adopted in this study are as follows (Duddeck and Erdmann 1985):

1. Two-dimensional plain-strain analysis are conducted for the tunnel lining and ground, assuming that loading along tunnel length, tunnel structures and ground condition are uniform.
2. The soil and the tunnel lining are treated as linear elastic materials
3. The soil stresses are assumed to be equal to the primary stress-state.
4. The tunnel lining-ground interaction are represented with bedding springs, i.e. radial springs and tangential springs.

4.0 DEVELOPING A FRAMEWORK FOR BEDDED-BEAM SPRING MODEL

4.1 The Framework

The authors reviewed the existing bedded-beam spring approaches developed over the years (Table 1) and documented a framework that incorporates 4 main steps: (1) Geometric definition of the tunnel lining (2) Boundary conditions application (3) Load application (4) Analysis definition. At the end of the analysis is a hold point that asks a critical question "Is the structural behaviour of the model realistic?". If not, then step (1) to (4) should be reviewed to ensure the inputs are appropriate as the structural model is just a design-supporting tool that generates outputs based on the simulation inputs and decisions. It is envisioned that this framework will improve the quality and efficiency on the modelling of bedded-beam spring model and thus be helpful to the practicing engineers embark on tunneling projects.

4.2 Lining Model

The simplest way to create an analytical model of a tunnel is to use beam elements which is available in most of the software in the engineering industry. The lining is discretized into series of individual beam elements. The depth of the beam would be the tunnel segment thickness while the width shall be taken as 1 meter for analysis carried out in per meter run manner. The beam elements are based on Bernoulli theory which do not take shear deformation into account and the cross-sections remain plane.

In STAAD Pro, the bedded-beam spring model is modelled at the centroidal circumference of the tunnel lining. It should be noted that the number of elements required depends on the tunnel size. A good practice of modelling the circumferential nodes would be keeping the overall number of nodes divisible by 360. For accurate representation of the lining, the rule of thumb is to space the circumferential nodes not to be greater than 350 mm to provide a smooth variation of internal forces induced in the tunnel lining and to capture steep forces variation if present. The local coordinate system of the beams shall be consistent in the structural model and this can be performed via the beam circular repeat option in STAAD Pro during beams generation to avoid unnecessary errors during load application in the later stage. An example of Second Heinenoord Tunnel structural model in STAAD is illustrated in Figure 6.

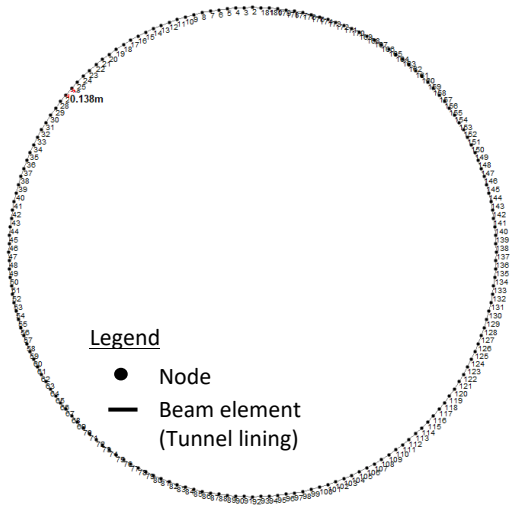

Figure 6 Structural model of Second Heinenoord Tunnel Circumferential nodes (node spacing 138 mm)

4.3 Boundary Conditions

Since the structural model is modelled as a 2D slice, there should be no concern in the out-of plane direction. The bending moment developed in the tunnel depends greatly on the relationship between deformation of the tunnel lining and the deformation of the soil medium. This principle is achieved by replacing the soil medium with springs around the tunnel segmental lining with: (i) Radial spring represents the passive subgrade reaction (ii) Tangential springs represents shear transmission at the soil-structure interface.

It is of crucial importance to note that the radial springs are non-tension springs as the soil would not be pulling on the tunnel segmental lining. In some commercial software whereby the compression only springs or elements are not available, this would require an iterative approach to manually remove those radial springs or elements which pick up the tensile force after running the analysis and re-run the analysis again. In STAAD Pro, the springs are modelled as inclined supports with respect to the center of tunnel with: (i) Radial springs in the global x-direction (ii) Tangential springs in the global y-direction. To allow automatic disconnection on the tension springs, a feature known as compression only springs in STAAD Pro could be assigned to the radial springs defined in the previous step (Figure 7).

A general practice to simplify the springs behavior is to assume the ground is linear elastic as the non-linear behaviour would require calibration from the geotechnical software or laboratory test. The stiffness of the radial spring adopted in this study is derived based on the empirical formula proposed by Duddeck and Erdmann (1985) given in Eq. 1. Paul et al. (1983) suggested the tangential spring stiffness with a value of near 20 percent of the radial springs is appropriate for smooth interface and up to 50 percent of the radial springs is appropriate for a rougher surface with irregular overbreak. The calculated springs stiffnesses should be multiplied with 1 m (per meter run analysis) and the node spacing before assigned to each node in the structural model.

$$K_r = \frac{E(1-v)}{(1+v)(1-2v)R} \quad (1)$$

Where E, v and R are the elastic modulus of soil, poisson's ratio of soil and centroidal radius of the tunnel respectively.

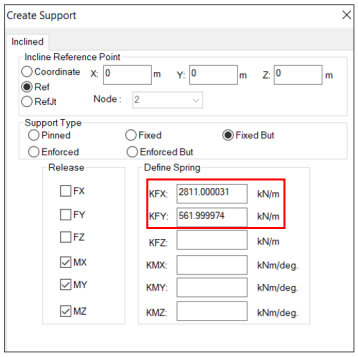

(a)

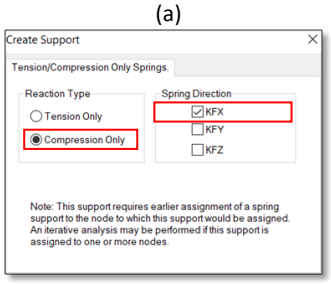

(b)

Figure 7 STAAD Pro springs definition – a) inclined support, b) support specification

4.4 Load Application

Having set up the bedded beam spring model, the main load cases applied to the bedded-beam spring structural model include ground load, groundwater pressure and surcharge. Although these are not the only loading conditions to be evaluated for, this section, however, is limited to the main load cases which the failure to withstand these load cases would give rise to an ultimate limit state (ULS) with major consequences [19]. The load application in STAAD Pro is simple if the local axes of the beam elements are consistent.

4.4.1 Ground Load

Hashimoto et al. (2002) has shown that the earth pressures acting on the tunnel lining do not revert to the primary state before tunneling which however, the conservative approach and common practice is to design the lining to the primary undisturbed earth pressures before tunneling without any reduction on the earth pressures for soft ground condition (ITA Working Group No. 2 2000). In contrast to the loading conditions proposed by Duddeck and Erdmann (1985) which would not be realistic for shallow tunnels, the soil pressures have been calculated at every point of the tunnel in this study as follows (Ngan Vu et al. 2017):

$$\sigma_v' = \gamma'(H + R\cos\theta) \quad (2)$$

$$\sigma_h' = K\gamma'(H + R\cos\theta) \quad (3)$$

Here σ'_v, σ'_h, H, γ', R, θ and K are the vertical earth pressure, horizontal earth pressure, height of overburden pressure, the submerged unit weight of the soil, tunnel radius, angle subtended between the element axis and the vertical axis of tunnel section and lateral earth pressure coefficient. The earth pressures are applied as vertical and horizontal projected member loads to the beam elements in STAAD Pro. The projected loads are applied and interpolated automatically along the global axis in the software by specifying the magnitudes and direction of the loads at the minimum and maximum global axis (see Figure 8b and Figure 8c).

4.4.2 Groundwater Load

The groundwater pressure acts on the tunnel lining as hydrostatic pressure. The resultant of the hydrostatic pressures at the tunnel crown and invert results in buoyancy. This will induce subgrade reactions, either at the crown or invert depending on the resultant pressures of the buoyancy and vertical earth pressure, surcharge and self-weight of tunnel. The groundwater pressure is applied as hydrostatically distributed member loads with the auto-interpolation function in STAAD Pro (see Figure 8a).

4.4.3 Surcharge

When there is surcharge on the ground surface, either due to traffic load, existing building or unknown future development, the increase in earth pressure acting on the tunnel segmental lining has to be accounted for. Similar to ground load, surcharge is applied as vertical and horizontal projected member loads (see Figure 8b and Figure 8c).

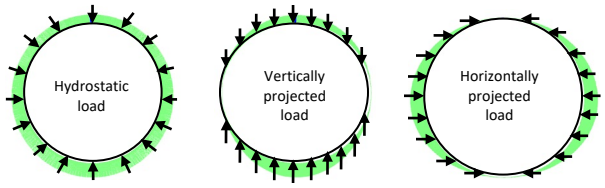

(a) (b) (c)

Figure 8 Loading application in STAAD Pro: a) Hydrostatic load - ground water load, b) vertical projected load - ground load and surcharge, c) horizontal projected load - ground load and surcharge

4.5 Segmental Joint (Radial Joints)

The flexural rigidity of joint, in reality is smaller than the flexural rigidity of the segments due to its reduced contact width to cater for gasket groove and caulking groove as a provision for leakage. To account for this, either indirect-joint model with correction on the overall lining flexural rigidity or direct-joint model with explicit simulation of the joints could be adopted. In this study, these 2 models have been considered and discussed in

comparison to better understand if the modelling responses are adequate in the context of the structural behaviours.

4.5.1 Direct-joint method - monolithic ring (Muir Wood 1975)

This modelling approach is achieved by correcting the overall ring flexural stiffness calculated by:

$$I_{eq} = I_{joint} + I_{full}(\frac{4}{n})^2 \leq I_{full} \quad (4)$$

Where I_{joint} is the moment of inertia of segment radial joint; I_{full} is the moment of inertia of full segment thickness; n is the number of main segments (excluding key segment). In the case studies, since the geometric specification of the radial joints are not available, they have been assumed to be 80% of the segment lining thickness given in Table 2 and Table 4. A simple relationship has been developed based on this assumption in Figure 9. It can be seen that with only 5 number of standard segments, the tunnel segmental lining of the reference project 2 has attained full flexural modulus as if there is no joints in the lining. Further reduction in the number of standard segments would not bring about any changes on the flexural modulus. Reference project 1 with 6+1 ring configuration, on the other hand, is shown to have lower flexural modulus. In STAAD Pro, this could be implemented by back- calculating the equivalent segment thickness from the corresponding flexural modulus.

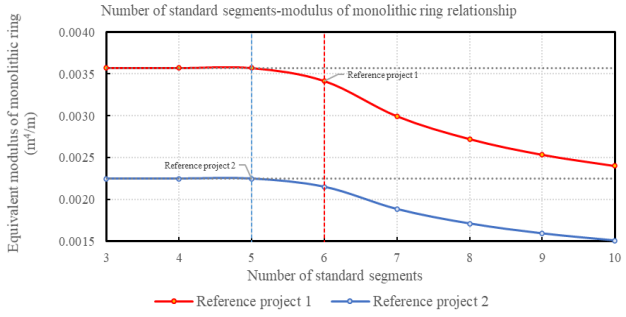

Figure 9 Relationship of number of standard segments with the equivalent flexural modulus of monolithic ring for the reference projects at 80% joint thickness

4.5.1 Direct-Joint Method – Segmented Ring

Direct-joint method regards the tunnel lining as a multiple-hinged ring model. The hinge is essentially semi-hinge with rotational stiffness determined according based on concrete hinge theory according to Leonhardt and Reimann [24] as:

$$k_\theta = \frac{9}{8} E_c a^2 m(1-2m)^2 \quad (5)$$

$$m = \frac{M}{N_{avg} a} \quad (6)$$

Here k_θ, E_c, a, m, N_{avg} and M represent rotational spring stiffness, Young's modulus of concrete, joint thickness, eccentricity ratio, average axial force and bending moment respectively. The bending moment-rotation relationship has been derived according to k_θ whereby the maximum bending moment across the joint is being capped at the plain concrete bending moment capacity, M_{yield}. M_{yield} of the plain concrete should be calculated from the average axial force of the tunnel lining. N_{avg} can be estimated based on the following expression [11]:

$$N_{avg} = \sigma_{v,axis} R \quad (7)$$

Where $\sigma_{v,axis}$ is the soil pressures at tunnel axis level. Instead of utilizing the plain concrete bending moment capacity, Do, et al. [25] assumed the bending moment corresponding to maximum permissible joint rotation, θ of 0.01 radians to be M_{yield}.

When the bending moment at the joint increases until full contact is no longer present, the joint will open and non-linearity relation between bending moment and rotation should occur [26]. By middle-third rule, this transition between linearity and non-linearity occurs theoretically at:

$$M_{linear} = \frac{N_{avg} a}{6} \quad (8)$$

where M_{linear} is the bending moment limit for linearity portion; N_{avg} is the average hoop force across the joint; and a is the joint thickness. With all the aforementioned information: (i) Mlinear - linear branch (ii) Post M_{linear} - joint softening behaviour (iii) M_{yield} - Moment capacity of concrete beyond which eternal rotation of joint would take place, a bending moment- rotation relationship can be described graphically as shown in Figure 10. Herein rotational spring stiffness is simply the slope of the curve. For simplification purposes, Do, et al. [25] approximated the rotational stiffness with a bilinear relationship by applying a factor of 0.8 applied to the eccentricity ratio and M_{yield}. The rotational stiffness is then applied to all the joints present in the tunnel lining. Using the similar concept, the authors improved the curve fitting with $0.7M_{yield}$ in this research to avoid underestimation on the stiffness of the joints, thus the bending moment transmitted across the joints especially at the ascending portion of the curve.

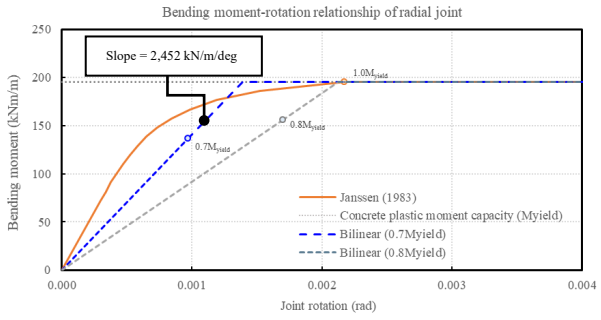

Figure 10 Bending moment-rotation relationship of radial joint (reference project 1)

In STAAD Pro, the rotational springs are specified as member released with rotational stiffness at the starts and ends of the beam members located at the joints (Figure 11).

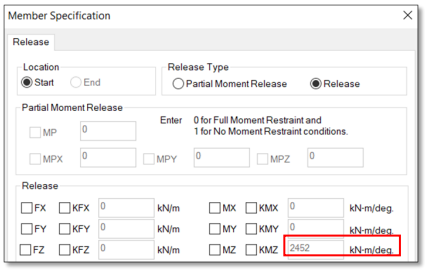

Figure 11 Member released with rotational spring in STAAD Pro.

4.6 Structural Analysis Definition

Structural analysis of the tunnel lining involves non-linearities of the springs. Thus, it is technically inaccurate to instruct the software to analyze the load cases by using load combination. Load combination combines the results obtained from the independent analysis of the individual load cases instead of analyzing the loads as if they are acting concurrently. This will result in wrong reactions reflected on the radial springs. Here, it should be emphasized that ''non-linearities'' in the software is only related for the springs as the radial springs in tension should be disconnected (one-way spring). It does not involve material non-linearity nor any effect of geometric non-linearity.

In STAAD Pro, repeat loads shall be generated whereby the displacements are computed based on the stiffness matrix and the load vector. In simple terms, the structure will be analyzed for the combination of loads rather than just combining the results.

4.7 Potential Implication of Framework

With the technical justification and clear description in the context of bedded-beam spring modelling, the framework directs the engineers to identify the key parameters and modelling features in STAAD Pro. In instances where only preliminary analysis is needed, some of the steps in the framework could be fit-for-purpose by further simplification based on engineering judgment. With adherence to the framework, the authors envision that the modelling efficiency, accuracy of the bedded-beam spring structural model could be improved and applied to tunneling projects. It is important to note that some of the modelling parameters are project-specific, careful consideration should be given during the process. The key recommendations of the overall framework are summarized in Table 6.

Table 6 Modelling framework components and consideration

Framework component	Key considerations and questions
1. Setting up lining geometry	• Identify tunnel specifications (i.e. radius, segment thickness, tunnel configuration, Young's modulus of concrete) • Length of discretized beam elements < 350 mm • Number of circumferential nodes divisible by 360 • Consistent coordinate system definition
2. Boundary conditions	• Radial springs stiffness - compression only [11] • Tangential springs stiffness - tension and compression [17] • Inclined spring supports with compression only spring specification in STAAD Pro • Check the reference point of the supports in STAAD Pro
3. Load cases and application	• Primary load cases (self-weight, earth pressure, groundwater pressure, surcharge) • Global projected load - earth pressure, surcharge • Hydrostatic load – groundwater pressure
4. Radial joints modelling options	• Identify segmental joint effective thickness (allowance for caulking groove, gasket groove) • Direct-joint method (monolithic ring) - [9] *Calculate overall reduced lining stiffness. Only consider number of standard segments for the reduction.* • Direct-joint method (segmented ring) - [26] *Explicit modeling of joints. Identify bending moment capacity of concrete under axial force. Calculation of rotational stiffness from the slope of bilinear curve. Member ends and starts should be moment-released with rotational stiffness.*
5. Analysis and post-analysis review	• Utilize repeat load in STAAD Pro (combination of loads, not combining results from individual load cases) • Is the model rotating? *If relevant, check if the loads have been applied symmetrically.* • Is the model unstable? *If relevant, check the out-of plane degree of freedom of the model.* • Is the lining deflected shape appropriate/ as expected? *Check the exaggerated deflected shape. With the ratio of vertical to horizontal loads applied, ovalization shape of the lining can be predicted.* • Are the reactions of the springs appropriate? *The reactions by logically definition should also be symmetrical.*

5.0 MODEL VALIDATION IN COMPARISON TO CASE STUDIES

In order to validate the bedded-beam spring model developed according to the framework in this study, structural models of the case studies have been made to allow comparison of the analytical results with the available data. Do, et al. [25] studied the critical joint orientations based on different joint numbers of the tunnel in which, 6-joint lining and 7-joint lining are most related to this study. It is noteworthy that, however, the study is most applicable for tunnel constructed by standard segments of similar size. The influence of key segment (the smallest segment in the tunnel) was not included. Thus, in this study, a simplified assumption was made by avoiding joints to be located at the tunnel crown (Figure 12), which is believed to be the highest bending moment location in the structural models. For comparison, ultimate limit state, ULS and serviceability limit state, SLS load combinations (LC) have been generated from the

main load cases on the basis of Eurocode which is widely adopted in many countries as shown in Table 7 [27].

Table 7 ULS load combinations [28]

Load cases	ULS load combinations		
	LC1	LC2	LC3
	Partial load factors		
Self-weight	1.35	1.35	1.35
Ground load	1.35	-	-
(low groundwater level)			
Ground load (groundwater level at ground level)	-	1.35	-
Ground load (groundwater level at floor level)	-	-	1.00
Groundwater load	1.35	-	1.35
(low groundwater level)			
Groundwater load (groundwater level at ground level)	-	1.35	-
Groundwater load (groundwater level at flood level)	-	-	1.35
Surcharge	1.5	1.5	-

Note: SLS load factors are taken to be 1.0 for all load cases.

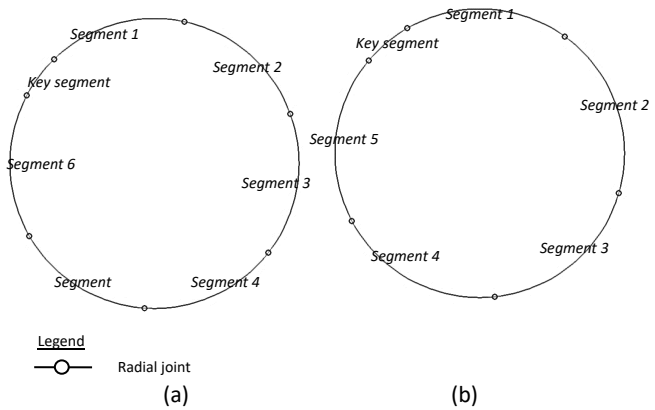

Figure 12 Joint orientations of a) Reference project 1 - Second Heinenoord Tunnel b) Reference project 2 - Ho Chi Minh Metro (HCMC) Line 1

Taking advantage of the presented models, i.e. indirect-joint model and joint-model, the remainder of this chapter is devoted to the discussion of the analysis results with the field measurements and design results for comparison and verification.

5.1 Results And Discussion (Reference Project 1 – Second Heinenoord Tunnel In Netherland)

The ULS and SLS analysis results are compared to the field measurement taken at the North Bank of Second Heinenoord Tunnel after 330 days. The monitoring results in Figure 12 are reproduced by the authors in for a direct comparison.

The derived bending moments from the analytical models are compared to the field measurements as shown in Figure 13. The figures indicate that the structural models are capable to derive the bending moment trend in the lining as compared to the field measurements. On the average, the analytical models are able to give a good indication of the stress distribution in the tunnel lining, wherein higher correlation is shown from the SLS results. Although the highest bending moment of the field measurement (20° on the cross-section of the tunnel lining) might be interpreted as an outlier, the maximum bending moment of the analytical results shows agreements for both segmented ring and monolithic ring. It is noticed that the highest bending moments of the analytical models are located at the tunnel invert (180°) which is in good agreement with the analytical models of Ngan Vu, et al. [14]. The comparison of the joints consideration approaches also suggested that simplified monolithic ring provokes an increase in maximum bending moment of the lining by about 22% compared to the segmented ring.

To begin with the evaluation of the axial forces, here our attention is drawn to the highly fluctuated field measurement that the analytical solutions do not seem to fit adequately with the measurements. Nearly half of the measured axial forces are lower than the expected axial forces generated in the tunnel lining (Figure 14). This can be attributed to, on the one hand, the accuracy of the soil pressure gauge is unclear, on the other hand, the influence of grout injection pressure was not taken into account at the measured time of 330 days [14, 19]. The SLS results of the analytical models, both monolithic and segmented rings tend to be lower than some of the field measurements. These scenario was recently explained by Ngan Vu, et al. [14] and the analytical results were shown to be even lower in Bakker's comparative study [19].

In contrast, the maximum measured axial forces are still well within the ULS analytical results which indicates that the structural model still provides a reasonable approximation on the ultimate designed hoop thrust. It is also worth noted that the difference in axial force is not noticeable regardless of the models in terms of consideration of the radial joints.

On the basis of this comparison, the analytical results of the bedded-beam spring model adopting the modelling framework have the highest conformity to the bending moments of the field measurements. The distribution of bending moments indicates similar trend as the field measurements with closely-match bending moments. The axial forces comparison, on the other hand, there exists disparity due to the field measurement accuracy. Overall, the ULS analytical results were also shown to be effective in determining the ultimate forces of the reference project.

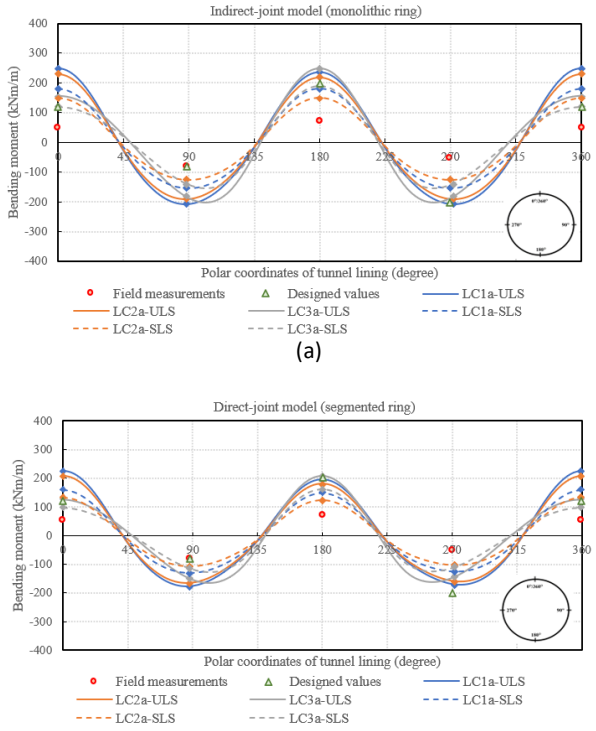

Figure 13 Bending moment validation of a) Indirect-joint model b) Direct-joint model for reference project 2

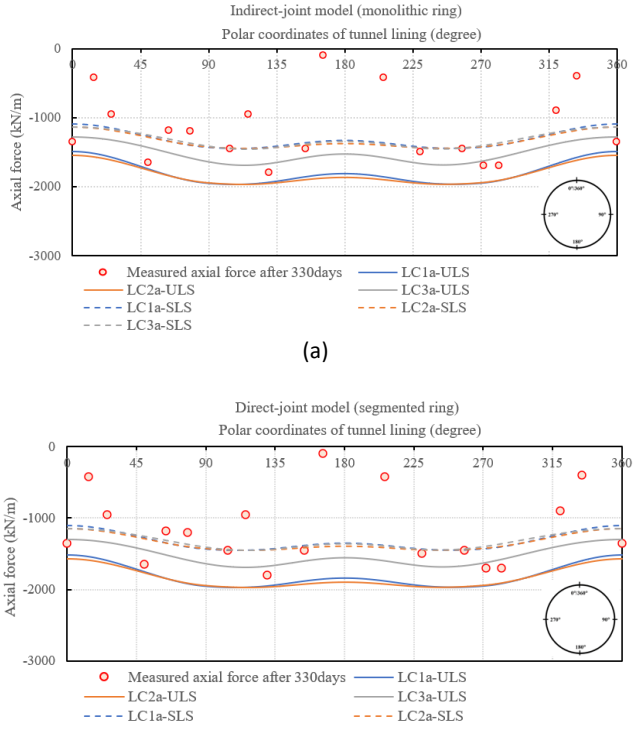

Figure 14 Axial force validation of a) Indirect-joint model b) Direct-joint model for reference project 1

5.2 Results And Discussion (Reference Project 2 - Ho Chi Minh Metro Line 1 In Vietnam)

In order to validate the presented deterministic model, analyses have been performed to derive the internal force of the tunnel lining of Ho Chi Minh City Metro Line 1. The published field measurement and the designed forces in Figure 14 have been reproduced in this section for comparison.

Comparison of bending moments presented in Figure 15 have shown that the trend of the bending moments are well-portrayed by the analytical results. In comparison with the field measurement, both SLS and ULS results indicate higher maximum bending moments which however, these results are in good agreements with the design values. Although the bending moments of the direct-joint model at 270° is slightly lower than the design results, it seems reasonable because this can be attributed to the different joint orientations considered by the authors in this study and the design consideration of the reference project. Besides, it was also observed that the monolithic ring exhibits a maximum difference of 18% in terms of the higher maximum bending moments compared to that of the segmented ring.

To begin with the comparison of the axial forces, here the attention should be first paid to the comparison between field measurement and design results of Kuriki (2020) in Figure 16. It can be seen that the trend of the field measurement is inconsistent whereby at the tunnel axis level (90° and 270°), great disparity could be observed. In addition, the relative differences between design results and field measurements are inconsistent. The reason for this was not clearly mentioned and examined so far but may be sought in the fact that the accuracy of the field measurement was unclear. The design results, including partial load factors in the calculation should show higher axial forces than the field measurement, both locally and globally. Otherwise, this would simply indicate underestimation in the design process.

Comparing the analytical results of the presented models, overall, the results display similar tendency of the distribution of axial forces that agree well with the design results. In terms of the magnitude of the internal forces, it can be seen that the results are quite consistent with each other with minor differences. By inspecting the field data points, one of the field data points matches the LC3-SLS curve. In the analytical model, it can be seen that under LC1 and LC2, the tunnel lining exhibits higher axial forces compared to LC3 due to the inclusion of surcharge. This might also explain the difference in the magnitude of axial force of tunnel lining under LC1 and LC2 are higher than the field measurements in both ULS and SLS plots.

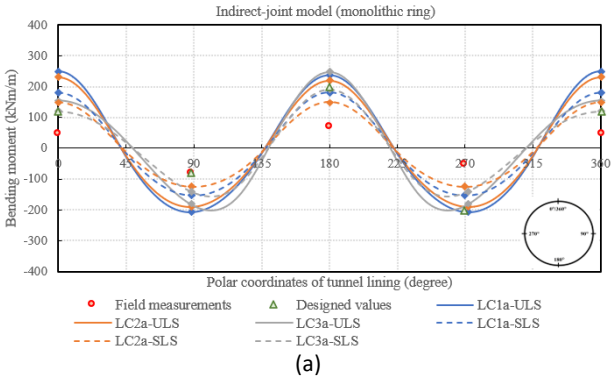

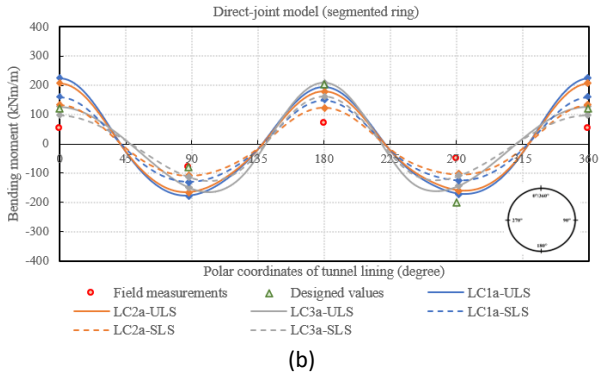

(b)

Figure 15 Bending moment validation of a) Indirect-joint model b) Direct-joint model for reference project 2

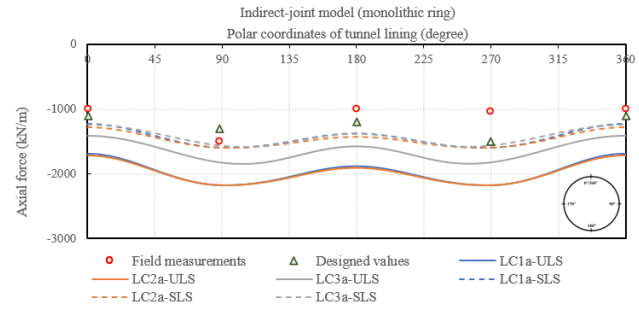

(a)

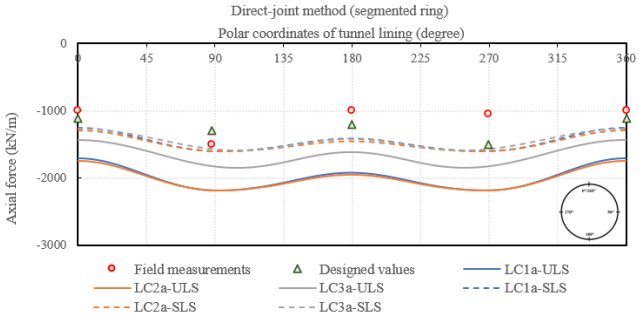

(b)

Figure 16 Axial force validation of a) Indirect-joint model b) Direct-joint model for reference project 2

Table 8 and Table 9 representatively summarize the comparison results of the case studies. Overall, the differences between the results in terms of bending moments and axial forces with the field measurement data can also be attributed to the volume loss during tunneling that causes soil relaxation between the ground and the tunnel lining. One has to consider in reality, tunneling affects the at-rest state of the soil and the total ground pressure acting on the tunnel lining is less than the designed full overburden pressure adopted in the structural models [21]. This can also explain why most of SLS analytical results are higher than the field measurements excluding the measurement outliers. On the basis of performance evaluation, both quantitively and qualitatively, it is shown that the deterministic analytical bedded-beam spring models in STAAD Pro developed according the proposed modelling framework is able to give good agreement with the field data and designed forces in terms of the trend of the forces and the maximum forces. It is noteworthy that the trend of the forces, as the most important indicator of validation was compared in all cases and good agreements with the analytical models signify the accurate structural response of the analytical models. On the average, the designed forces are closer to the ULS analytical results whereas the field measurements correlate better with the SLS analytical results. The analytical models permit a reasonable and conservative estimation of the SLS and ULS forces in the tunnel lining for the reference projects.

Table 8 Maximum bending moment comparison (field measurements, design results and analysis results)

Bending moment comparison (reference project 1)							
Load combination	**Field measurements**	**Design results**	**Monolithic ring**	**Segmented ring**	**$M_{max,\ mono}$/ $M_{max,\ field}$**	**$M_{max,\ mono}$/ $M_{max,\ design}$**	**$M_{max,\ mono}$/ $M_{max,\ seg}$**
	$M_{max,\ field}$	**$M_{max,\ design}$**	**$M_{max,\ mono}$**	**$M_{max,\ seg}$**			**R_M**
	kNm/m	**kNm/m**	**kNm/m**	**kNm/m**	-	-	-
LC1-ULS	200	-	209.8	170.8	1.05	-	1.23
LC2-ULS			171.2	133.9	0.86	-	1.28
LC3-ULS			229.3	196.0	1.15	-	1.17
LC1-SLS			161.7	132.9	0.81	-	1.22
LC2-SLS			126.9	105.3	0.63	-	1.20
LC3-SLS			178.7	153.3	0.89	-	1.17

Bending moment comparison (reference project 2)							
Load combination	**Field measurements**	**Design results**	**Monolithic ring**	**Segmented ring**	**$M_{max,\ mono}$/ $M_{max,\ field}$**	**$M_{max,\ mono}$/ $M_{max,\ design}$**	**$M_{max,\ mono}$/ $M_{max,\ seg}$**
	$M_{max,\ field}$	**$M_{max,\ design}$**	**$M_{max,\ mono}$**	**$M_{max,\ seg}$**			**R_M**
	kNm/m	**kNm/m**	**kNm/m**	**kNm/m**	**-**	**-**	**-**
LC1-ULS	80	200	249.4	224.9	3.12	1.25	1.11
LC2-ULS			229.9	207.2	2.59	1.15	1.11
LC3-ULS			248.0	209.8	3.10	1.24	1.18
LC1-SLS			180.5	160.3	2.26	0.90	1.13
LC2-SLS			149.2	132.4	1.87	0.75	1.13
LC3-SLS			190.0	161.1	2.38	0.95	1.18

Table 9 Maximum axial force comparison (field measurements, design results and analysis results)

Axial force comparison (reference project 1)							
Load combination	**Field measurements**	**Design results**	**Monolithic ring**	**Segmented ring**	**$N_{max,\ mono}$/ $N_{max,\ field}$**	**$N_{max,\ mono}$/ $N_{max,\ design}$**	**$N_{max,\ mono}$/ $N_{max,\ seg}$**
	$N_{max,\ field}$	**$N_{max,\ design}$**	**$N_{max,\ mono}$**	**$N_{max,\ seg}$**	**-**	**-**	**R_N**
	kN/m	**kN/m**	**kN/m**	**kN/m**	**-**	**-**	**-**
LC1-ULS	1,800.0	-	1,966.0	1,975.6	1.09	-	1.00
LC2-ULS			1,965.5	1,974.0	1.09	-	1.00
LC3-ULS			1,686.2	1,691.3	0.94	-	1.00
LC1-SLS			1448.3	1,455.0	0.80	-	1.00
LC2-SLS			1449.8	1,455.3	0.81	-	1.00
LC3-SLS			1453.0[1]	1,456.9[1]	0.81	-	1.00
Axial force comparison (reference project 2)							
Load combination	**Field measurements**	**Design results**	**Monolithic ring**	**Segmented ring**	**$N_{max,\ mono}$/ $N_{max,\ field}$**	**$N_{max,\ mono}$/ $N_{max,\ design}$**	**$N_{max,\ mono}$/ $N_{max,\ seg}$**
	$N_{max,\ field}$	**$N_{max,\ design}$**	**$N_{max,\ mono}$**	**$N_{max,\ seg}$**	**-**	**-**	**R_N**
	kN/m	**kN/m**	**kN/m**	**kN/m**	**-**	**-**	**-**
LC1-ULS	1,500.0	1,500.0	2,175.0	2,181.2	1.45	1.45	1.00
LC2-ULS			2,172.5	2,178.2	1.45	1.45	1.00
LC3-ULS			1,842.5	1,845.2	1.23	1.23	1.00
LC1-SLS			1,599.4	1,604.2	1.07	1.07	1.00
LC2-SLS			1,595.5	1,599.4	1.06	1.06	1.00
LC3-SLS			1,578.9[2]	1,580.7[2]	1.05	1.05	1.00

Quick verification on hoop force:

[1]Reference project 1: LC3-SLS: Ground cover to tunnel axis: 16.1 m; average effective unit weight: 11.7 kN/m³; radius: 4.14 m
Back calculated average hoop force: [(16.1 x 10) + (11.7 x 16.1)] x 4.14 m = 1,446 kN/m

[2]Reference project 2: LC3-SLS: Ground cover to tunnel axis: 23.1 m; average effective unit weight: 9.9 kN/m³; radius: 3.325 m
Back calculated average hoop force: [(23.1 x 10) + (9.9 x 23.1)] x 3.325 m = 1,528 kN/m

6.0 PARAMETRIC STUDY

The validated models have demonstrated a scenario which is worthy of in-depth investigation; that is, the monolithic ring (indirect-joint method) has always shown greater maximum bending moments compared to segmented ring (direct-joint method) in the validation process. For the investigation of the parametric responses, two important elasticity ratios: (i) flexibility ratio, α and (ii) compressibility ratio, β proposed by Duddeck and Erdmann [11] were introduced and studied in parallel with the lateral earth pressure coefficient, *K*. The elasticity ratios can be calculated by:

$$\alpha = \frac{ER^3}{E_c I} \tag{9}$$

$$\beta = \frac{ER}{E_c A} \tag{10}$$

Here *I* denotes the moment of inertia of tunnel lining depending on the approach to consider the presence of radial joints (I_{eq} for monolithic ring; I_{full} for segmented ring) and *A* denotes the cross-sectional area of the lining. Based on these ratios, if the soil medium is relatively weak or the tunnel lining is relatively stiff, the lining tends to exhibit greater bending moment and hoop force [11]. The validated models of reference project 1 were used in this study and the α and β of

the tunnel segmental lining have been calculated over a soil elastic modulus range from 1.2 MPa to 3000 MPa respectively (Table 10). For clarity purpose, the results obtained from the parametric studies are plotted only up to E_s = 600 MPa (upper bound) with a line at E_s = 10 MPa indicating the lower bound, corresponding to the elastic modulus of soft rocks and soft soils respectively to represent the applicable range of this study.

Table 10 Tunnel flexibility ratio and compressibility

Soil elastic modulus E_s	Flexibility ratio α		Compressibility ratio β	
MPa	Monolithic ring	Segmented ring	Monolithic ring	Segmented ring
1.2	0.59	0.57	0.0004	0.0004
2.4	1.18	1.13	0.0007	0.0007
12	5.91	5.66	0.0037	0.0037
24	11.82	11.32	0.0073	0.0075
36	17.72	16.97	0.0110	0.0112
48	23.63	22.63	0.0147	0.0149
60*	29.54	28.29	0.0184	0.0186
300	147.70	141.46	0.0919	0.0932
600	295.40	282.92	0.1837	0.1864
1200	590.79	565.83	0.3674	0.3727
3000	1476.97	14114.58	0.9185	0.9318

Note: "*" denotes soil elastic modulus of reference project 1

6.1 Influence Of Lateral Earth Pressure And Tunnel Flexibility Ratio On Bending Moment

Most of the studies have been focusing on the response of tunnel segmental lining under different lateral earth pressure coefficient, *K* values at 0.5 intervals and a great deal of useful information have been obtained. Thus, in this study, the effect of *K* on the tunnel lining performance is investigated by adopting the bedded-beam spring models of project reference 1 and much attention was given to the lateral earth pressure coefficients, *K* equal and less than 1.0, i.e. *K* of 0.1, 0.3, 0.5, 0.8 and 1.0 over the range of flexibility ratios listed in Table 10.

In Figure 17a generally, the bending moments developed in the tunnel lining for both monolithic and segmented ring are sensitive to the α, especially at low range from 5 to 30. Beyond an α value of 30, the changes in the maximum bending moment become more gradual and the curves flatten at α of 200. With higher lateral earth pressure, it is expected that the magnitude of maximum bending moment induced in the tunnel lining is smaller than that of *K* = 0.5, and vice versa, higher bending moments when *K* = 0.1 and 0.3. The bending moment was thought to be the lowest when the lateral earth pressure coefficient is at unity. Either increase of decrease, leads to an increase in bending moment due to vertical and lateral earth pressure difference. However, it should be mentioned that *K* = 1.0 yields higher bending moment compared to *K* = 0.8. This phenomenon could be explained by the tendency of tunnel lining ovalization. For *K* = 0.5 and 0.8, horizontal ovalization is expected as the overburden pressure is dominant and the tunnel has the tendency to flatten out. In contrast, at *K* = 1.0, the lateral earth pressure is dominant, thus leads to horizontal compression of the tunnel and vertical ovalization (Bakker and Blom, 2009). The maximum bending moment becomes greater when the difference between vertical and lateral pressures is more profound. By making a direct comparison between *K* = 0.8 and 1.0, *K* = 1.0 has shown higher differences. Thus, it is not surprising to reveal that under *K* = 1.0, the tunnel lining exhibit higher maximum bending moment than *K* = 0.8. These results are in good agreement with the ones obtained by Tien et al. (2020).

6.2 Bending Moment Ratio

The maximum bending moment ratio, R_M is defined as the ratio of maximum absolute bending moments in the tunnel lining induced in segmented ring to the corresponding values developed in the monolithic ring. In Figure 17b, the results have shown that at the lower bound of flexibility ratio, α = 5, the segmented linings developed up to 90% of the maximum bending moment induced in the monolithic ring for all *K* values. Beyond an α value of 30, the maximum moment ratio, R_M reduces to 0.8 and the reduction becomes more gradual and approaches R_M value of about 0.72 (*K* = 0.1, 0.3, 0.5) and 0.79 (*K* = 0.8) at the upper bound of E_S.

This trend, however, is not observed for *K* = 1.0 whereby the maximum bending moment ratio, R_M reduces from 0.9 (α = 5) to 0.87 (α = 30) and gradually increases to a maximum R_M value of 0.93. This can be explained by the transition of tendency in the direction of ovalization (Figure 18) and the locations of maximum bending moments developed in the tunnel lining as follows:

1. Unlike other *K* values, whereby the maximum bending moments are usually observed either at the tunnel crown and invert for all α values with horizontal ovalization (lateral earth pressure is always less than the overburden at every point, vertical displacement is more dominant); Under *K* = 1.0, the lateral earth pressure equals to the overburden at every point and the tunnel invert experiences the greatest inwards pressure.

2. At low α, the medium subgrade is too weak to restraint the vertical ovalization effect. The tunnel lining can be viewed as a free body diagram with attention given to the tunnel crown, axis and invert. In this case, the resultant inward forces increase from the tunnel crown to the tunnel invert; the tunnel invert experiences the greatest vertical pressures and vice versa, lowest at the tunnel crown. Under this circumstance, the tunnel lining tends to ovalize vertically with the highest displacement at the tunnel crown (lowest inward force) and with the maximum bending moment located at the tunnel invert (largest inward force).

3. While α increases to a value of 30, the resistance of subgrade to the vertical ovalization effect is more

prominent. At this instance, here is the transition: the horizontal diameter at tunnel spring line region shortens more than the vertical diameter. In other words, the horizontal displacement is now more significant than the vertical displacement due to the stiffer subgrade to restrict the tunnel from ovalizing vertically. The maximum bending moment location is shifted to the tunnel spring axis level.

4. Based on the joint orientation assumption (Figure 12a), it can be seen that there is a radial joint located close to the tunnel invert but not at the tunnel axis. When the maximum bending moments occur at the tunnel invert, the radial joints as rotational springs only allow partial moment transfer and thus, leading to lower bending moments and thus, lower R_M. On this basis, the reason for the transition of R_M is therefore the influence of the joint orientations, whether it coincides with where the maximum bending moment developed.

5. The explanation for this phenomenon is valid especially when the tunnel is shallow as the vertical pressures at the tunnel crown and invert are significantly different except for the case where the surcharge is very substantial.

Referring to all of the previously mentioned, it is possibly to conclude that, the ratios of maximum bending moment, R_M induced in segmented ring to the corresponding value developed in the monolithic ring are in the range from about 0.72 to 0.93. The adoption of monolithic ring without consideration of joints is still a conservative approach regardless of lateral earth pressure coefficient but the degree of conservatism depends on the flexibility ratio, α and the orientation of the joints considered.

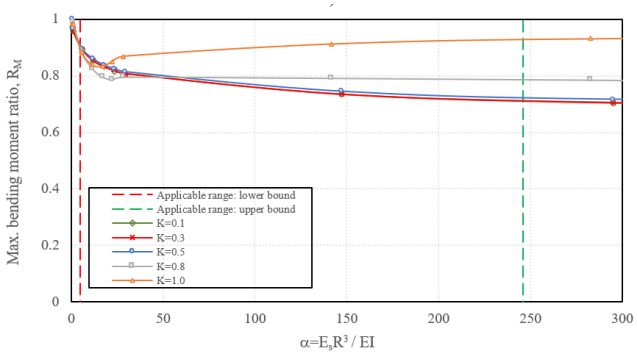

(a)

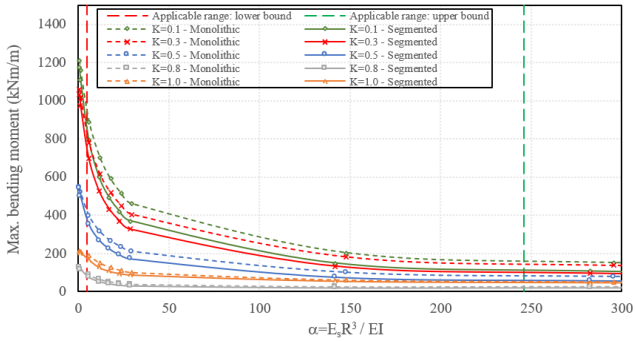

(b)

Figure 17 The variation of tunnel a) maximum bending moment b) bending moment ratio, R_M for different lateral earth pressure coefficient, K and tunnel flexibility ratio, α

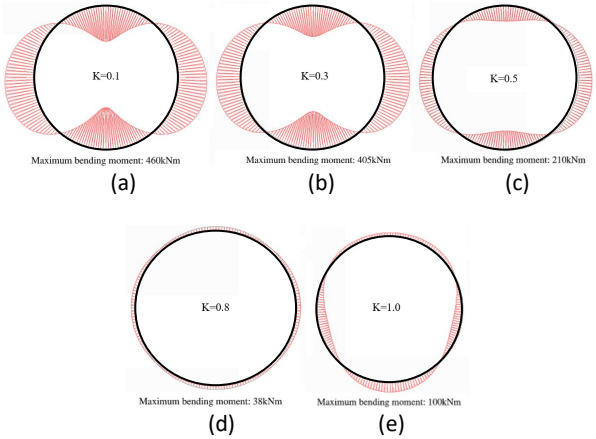

Figure 18 The variation of tunnel maximum bending moment for different lateral earth pressure coefficient, K at tunnel flexibility ratio, α = 29

6.3 Influence Of Lateral Earth Pressure And Tunnel Compressibility Ratio On Axial Force

Unlike bending moment, the axial force developed in the tunnel lining is not sensitive regardless of the approach to consider the radial joints, either through monolithic ring or segmented ring (Figure 19a). Generally, the increase in lateral earth pressure coefficient, K from 0.5 to 1.0 results in an increase in axial force of the tunnel lining within the compressibility ratio, β range between 0 to 0.15. These results agree well with the results presented by Do et al. (2013). However, by comparing the response of K = 0.1, 0.3 and 0.5, highest maximum axial force was found at K = 0.1, followed by K = 0.3 and K = 0.5 with very slight difference observed. For a more intuitive explanation on this contrary in trend, an example of the variation of axial force developed in the tunnel segmental lining was plotted in Figure 20. Generally, for K = 0.8 and K = 1.0, the tunnel segmental lining is associated with uniform axial force distribution with the maximum axial forces located at the tunnel invert. On the other hand, the axial forces for K = 0.1, 0.3 and 0.5 fluctuated significantly and the maximum axial forces are found to be at the tunnel axis.

6.4 Axial Force Ratio

The axial force ratio, R_N is defined as the ratio of the maximum absolute value of the axial force induced in a segmental ring to the value induced in a monolithic ring. Figure 19b shows that the normal force ratio, R_N is approximately equal to unity for all K values which indicates that there is no apparent influence with regards to the approach to consider the radial joints.

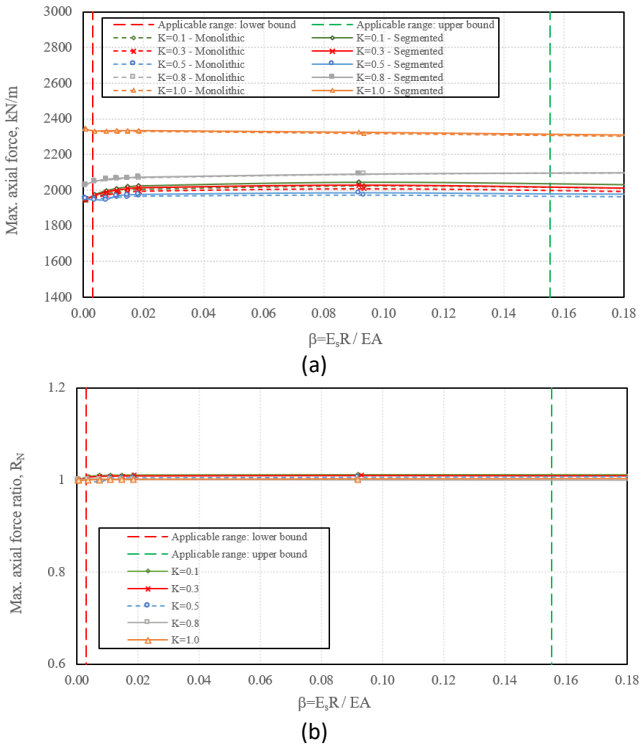

Figure 19 The varation of tunnel a) maximum axial force b) axial force ratio, R_N for different lateral earth pressure coefficient, K and tunnel compressibility ratio, β

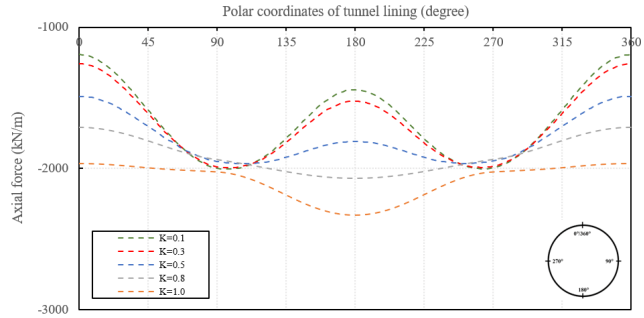

Figure 20 Variation of axial force for different lateral earth pressure coefficient, K at tunnel compressibility ratio, β = 0.0184

7.0 CONCLUSION

This study dealt with the analytical approach to the structural behaviour of tunnel segmental lining. A comprehensive modelling framework which is sufficiently prescriptive for the 2D bedded-beam spring model is presented in the paper, thereby ensuring the guidance for every specific step can be implemented in the structural model. Using the framework, bedded beam spring models were generated to verify against the field measurements and design values of 2 reference projects: (1) Second Heinenoord Tunnel in Netherland and (2) Ho Chi Minh Metro Line 1 in Vietnam. In the verification process, two approaches in considering the presence of radial joints: (1) monolithic ring and (ii) segmented ring were incorporated and the structural responses were compared and reviewed. It was shown that the distribution of the lining internal forces and the maximum designed forces were well-predicted. The ULS analytical results suggested better conformity to the designed forces; on the other hand, better correlations were shown between field measurements and the SLS analytical results. Additionally, adopting the monolithic ring results in higher maximum bending moment but with negligible influence on the axial force compared to the segmented ring. It was concluded that the framework is adequate in predicting the accurate modelling response that reflects the actual behavior of the tunnel segmental lining.

The verified models were then used to clarify the influence of the ground parameters on the response of the tunnel segmental lining. Given 12 different soil elastic moduli, E_S and 5 different lateral earth pressure coefficients, K, the tunnel flexibility ratio, α and compressibility ratio, β were calculated and the influence on the bending moments and axial forces developed in the tunnel segmental lining were carefully studied. As a result, the following was suggested:

1. Considerably reduction in the maximum bending moment was observed at α values from 5 to 30. Beyond α value of 30, the influence becomes more gradual and the curves flatten at α value of 200.

2. The effect of K on the maximum bending moment developed gradually reduces from K = 0.1 to K = 0.8, increases again when approaching K = 1.0 due to the change in ovalization direction and the increase in the differences between the vertical and lateral pressures in terms of magnitude.

3. It was again demonstrated that the monolithic ring yields higher maximum bending moment, with the maximum bending moment ratio, R_M between 0.72 to 0.93. The ratio is sensitive to the orientation of radial joints and location where the maximum bending moments developed.

4. The β values have negligible influence on the axial force developed in the tunnel lining.

5. There is no apparent difference in terms of maximum axial forces regardless of the approach to consider the radial joints under all parameters and the axial force ratio, R_N is close to unity.

It is envisaged that the presented modelling framework could be implemented for the design of segmental tunnel lining for actual tunneling projects based on the performance verification through the reference projects and the structural responses observed from the parametric study. For further studies, it is recommended that the influence of heterogenous soil

conditions on the development of tunnel internal forces could be investigated for different α, β and K. The critical joint orientations including the key segment shall be examined especially when the surcharge load is relatively significant.

Acknowledgement

The authors would like to acknowledge the technical supports received from Universiti Teknologi Malaysia (VOT Q.J130000.2409.09G33)

References

[1] Gruebl, F. 2006. Modern design aspects of segmental lining. in *CPT-ITA Congress*.

[2] Duddeck, H. and Erdmann, J. 1983. Structural design models for tunnels: Tunnelling 82, proceedings of the 3rd international symposium, Brighton, 7–11 June 1982, P83–91. Publ London: IMM, 1982, *International Journal of Rock Mechanics and Mining Sciences & Geomechanics Abstracts,* 20(1), p. A15, 1983/02/01/.

[3] Schmid, H. 1926. *Statische Probleme des Tunnel- und Druckstollenbaues und ihre gegenseitigen Beziehungen*. Berlin: Springer.

[4] Voellmy, A. 1937. Eingebettete rohre. ETH Zurich.

[5] Morgan, H. 1961. A contribution to the analysis of stress in a circular tunnel. *Geotechnique,* 11(1): 37-46.

[6] Schulze, H. and Duddeck, H. 1964. Spannungen in schildvorgetriebenen Tunneln. *Beton-und Stahlbetonbau,* 59(8): 169-175.

[7] Windels, R. 1966. Spannungstheorie zweiter Ordnung für den teilweise gebetteten Kreisring. Die Bautechnik 43 (1966), H. 8, S. 265–274.

[8] Windels, R. 1967. Kreisring im elastischen Kontinuum. *Der Bauingenieur Bd,* 4: 429.

[9] Muir Wood, A. 1975. The circular tunnel in elastic ground. *Géotechnique,* 25(1): 115-127.

[10] Muir Wood, A. 1976. Discussion: The circular tunnel in elastic ground. *Géotechnique.* 26(1) : 231-237.

[11] Duddeck, H. and Erdmann, J. 1985. Structural design models for tunnels in soft soil. *Underground Space;(United States),* vol. 9.

[12] Blom, . 2002. Design philosophy of concrete linings for tunnels in soft soils. TU Delft, *Delft University of Technology*.

[13] Oreste, P. 2007. A numerical approach to the hyperstatic reaction method for the dimensioning of tunnel supports. *Tunnelling and Underground space technology,* 22(2): 85-205.

[14] Ngan Vu, M., Broere, W. and Bosch, J.W. 2017. Structural analysis for shallow tunnels in soft soils. *International Journal of Geomechanics,* 17(8): 04017038.

[15] Zlatanović, E., Šešov, V., Lukić, D. Č., Prokić, A., and Trajković-Milenković, M. 2017. Tunnel–ground interaction analysis: Discrete beam–spring vs. continuous fe model. *Technical Gazette,* 24(1): 61-69.

[16] Guan, Z., Deng, T., Wang, G. and Jiang, Y. 2015. Studies on the key parameters in segmental lining design. *Journal of Rock Mechanics and Geotechnical Engineering,* 7(6): 674-683.

[17] Paul, S., Hendron, A., Cording, E., Sgouros, G. and Saha, P. 1983. Design Recommendations for Concrete Tunnel Linings: Volume II. Summary of Research and Proposed Recommendations. United States. Urban Mass Transportation Administration.

[18] Bakker, K. J. and Blom, C. 2009. Ultimate limit state design for linings of bored tunnels. *Geomechanics and Tunnelling,* 2(4): 345-358.

[19] Bakker, K. 2003. Structural design of linings for bored tunnels in soft ground. *Heron,* 48(1): 33-64.

[20] Bakker, K., Leendertse, W., JOVANOVIC, P. and VAN OOSTERHOUT, G. C. 2000. Monitoring: Evaluation of stresses in lining of the Second Heinenoord Tunnel. in *Geotechnical aspects of underground construction on soft ground*, 197-202.

[21] Hashimoto, T., Nagaya, J., Konda, T. and Tamura, T. 2002. Observation of lining pressure due to shield tunneling. in *Geotechnical aspects of underground construction in soft ground*, 119-124.

[22] Kuriki, M. 2020. Design and construction of first bored tunnel under Ho Chi Minh City Metro Line 1 in Vietnam. *Geotechnics for Sustainable Infrastructure Development*, Singapore, 221-228: Springer Singapore.

[23] Hieu, N. T., Giao, P. H. and Phien-wej, N. 2020. Tunneling induced ground settlements in the first metro line of Ho Chi Minh City, Vietnam. in *Geotechnics for Sustainable Infrastructure Development*: Springer, 297-304.

[24] Leonhardt, F. and Reimann, H. 1965. *Betongelenke: Versuchsbericht; Vorschläge zur Bemessung und konstruktiven Ausbildung. Kritische Spannungszustände des Betons bei mehrachsiger, ruhender Kurzzeitbelastung*. Ernst.

[25] Do, N.A., Dias, D., Oreste, P. and Djeran-Maigre, I. 2013. 2D numerical investigation of segmental tunnel lining behavior. *Tunnelling and Underground Space Technology,* 37: 115-127.

[26] Janssen, P. 1983. Tragverhalten von Tunnelausbauten mit Gelenktübbings, Report-No. 83-41 University of Braunschweig, Department of civil engineering. *Institute for structural analysis*.

[27] British Standard Institution. 2002. Eurocode 0: Basis of structural design. *European Standard*.

[28] Swee, C., Dazhi, W., Hong, N.B. and Fok, P. 2010. Engineering Group Civil Design Criteria for Road and Rail Transit Systems.